Food Chemistry 455 (2024) 139944

Contents lists available at ScienceDirect

Food Chemistry

journal homepage: www.elsevier.com/locate/foodchem

Non-linear responses via agglomeration and aggregation of gold nanoparticles for surface-enhanced Raman spectroscopy (SERS) coupled with chemometric analysis for chlorpyrifos detection

Xiaotong Liu [a], Udit Pant [a], Natasha Logan [a], Qiqi He [a], Brett Greer [a], Christopher T. Elliott [a,c], Cuong Cao [a,b,*]

[a] Institute for Global Food Security, School of Biological Sciences, Queen's University Belfast, 19 Chlorine Gardens, Belfast, BT9 5DL, United Kingdom
[b] Material and Advanced Technologies for Healthcare, Queen's University of Belfast, – 18-30 Malone Road Belfast, BT9 5DL, United Kingdom
[c] School of Food Science and Technology, Faculty of Science and Technology, Thammasat University (Rangsit Campus), Khlong Luang, Pathum Thani 12120, Thailand

ARTICLE INFO

Keywords:
SERS
Chlorpyrifos
Gold nanoparticle
Agglomeration
Aggregation
Chemometric analysis

ABSTRACT

This study investigates the behaviour of gold nanoparticles (AuNPs) when exposed to chlorpyrifos, an agricultural pesticide, and its application in detecting the pesticide via surface-enhanced Raman spectroscopy (SERS). Under synergistic addition of NaCl, AuNPs undergo agglomeration at lower chlorpyrifos concentrations but aggregation at higher concentrations, resulting in a distinctive nonlinear SERS response. A linear relationship is obtained between 0.001 and 1 ppm with detection limit (LOD) of 0.009 ppm, while an inverse response is observed at higher concentrations (1–1000 ppm) with a LOD of 1 ppm. Combining the colorimetric response of AuNP solutions, their absorbance spectra, and principal component analysis can improve detection reliability. The assay, coupled with a simple recovery method using acetonitrile swabbing, achieves high reproducibility in detecting chlorpyrifos in cucumber, even at concentrations as low as 0.11 ppm. This approach can be tailored for various chlorpyrifos concentrations not only in cucumbers but also in different food matrices.

1. Introduction

In the past 50 years, global food production has tripled owing to the Green Revolution in the 1960s, boosting agricultural productivity through high-yielding crops in Latin America and Asia (Evenson & Gollin, 2003). A significant contributor to this growth was through the extensive use of pesticides, which act as a defence mechanism against diseases and pests (Tabibi & Jafari, 2022). Each year, >4 million tonnes of pesticides are used worldwide, with only a small portion (1–25%) reaching their intended target. Excess residues enter the environment, resulting in considerable contamination (Leskovac & Petrović, 2023). Additionally, there are significant global public health and environmental challenges associated with the misuse and overuse of pesticides.

Over 50% of insecticides used worldwide are organophosphorus (OPPs) compounds (Ore, Adeola, Bayode, Adedipe, & Nomngongo, 2023). Among the OPPs, chlorpyrifos (CPF) is of crucial importance in agriculture, but it is also extremely harmful to human health. It has adverse effects on cholinergic transmission in the nervous system through inhibition of acetylcholinesterase enzyme activity (Weerathunge et al., 2019). Additionally, excess concentrations of CPF have been linked to diseases such as cancer, neurotoxicity, mutagenicity, and endocrine disruption in humans (Zhao et al., 2023).

Owing to health and safety concerns, CPF has been banned in the UK (Parliament, 2021) and in the EU (EFSA, 2019) due to the adverse effects on cognitive function and neurological development in children. However, it cannot be ruled out that it may still be imported from or used in other countries. Therefore, devising a highly efficient, sensitive analytical method to detect even trace amounts and a wide range of CPF concentrations in environmental and agricultural samples is essential. Such a detection platform is vital for ensuring food safety and regulatory adherence, given that there is the potential for residues to persist in the environment and contaminate imported foods destined for countries with restrictions on its use (Schreinemachers et al., 2015).

Surface-enhanced Raman spectroscopy (SERS) is a powerful analytical technique extensively used in research areas such as analytical chemistry, food safety, and forensic science (Zhang et al., 2019). SERS is

* Corresponding author at: Institute for Global Food Security, School of Biological Sciences, Queen's University Belfast, 19 Chlorine Gardens, Belfast, BT9 5DL, United Kingdom.
E-mail address: c.cao@qub.ac.uk (C. Cao).

https://doi.org/10.1016/j.foodchem.2024.139944
Received 23 March 2024; Received in revised form 30 May 2024; Accepted 31 May 2024
Available online 3 June 2024

a vibrational spectroscopic technique that enhances Raman scattering by molecules adsorbed on or near metallic nanostructures (e.g. gold, silver, copper) (Malik et al., 2023). The enhancement is typically attributed to electromagnetic and chemical enhancement mechanisms, offering robust and specific molecular fingerprints with exceptional sensitivity (Langer et al., 2020). For enhancing SERS detection capabilities, gold nanoparticles (AuNPs) and silver nanoparticles (AgNPs) have been extensively investigated (Xiong et al., 2023; Zhu et al., 2018), including application for the detection of thiol-containing pesticides (Park et al., 2022). In addition, several studies have also reported on SERS-based detection of CPF as summarised in Table S1.

However, there is often a compromise between SERS sensitivity and the dynamic range of detection (Chang et al., 2016). For instance, tip-enhanced Raman spectroscopy (TERS) excels in detecting single molecules. It achieves this by sensing one or a few molecules in close proximity to locally enhanced electromagnetic fields generated on sub-nanometer nanostructures at the tips (Kang et al., 2022; Zrimsek et al., 2017). However, as analyte concentration increases, TERS faces challenges. This is primarily due to the saturation of the metallic nanosurfaces, making it difficult to accommodate excess analyte molecules. The saturation phenomenon means that higher concentrations do not yield proportionally higher Raman signals. Consequently, this constrains the dynamic range of the analytical method. Additionally, in the case of colloidal SERS substrates, such as colloidal AuNPs or AgNPs, SERS effectiveness is in harmony with the particles' agglomeration and aggregation. On the one hand, particle agglomeration and aggregation can reduce the interparticle distance, leading to the formation of stronger electromagnetic enhancement and increased hot spots (Chan, Leng, & Vikesland, 2018). This way, aggregating agents (e.g. NaCl, KCl, $MgCl_2$, Na_2SO_4, and $MgSO_4$) have been widely exploited in SERS analysis to further amplify the Raman signal (Cholula-Diaz et al., 2018; Ye et al., 2023). However, on the other hand, once the particles are completely aggregated, the formation of hot spots will be disrupted, leading to the diminishment of SERS intensity. This hinders the sensitive and accurate quantification of analyte concentrations across a wide range. Nanoparticles that aggregate unpredictably yield non-reproducible signals in SERS, restricting their use in various applications (Lu et al., 2021; Wang et al., 2023). Gaining insights into the states and behaviours of the agglomeration and aggregation is vital for determining their trajectory and dispersal in complex systems, assisting experimental optimisations to improve sensitivity and dynamic range of the SERS testing.

Herein, we report an interesting finding in which the agglomeration and aggregation of AuNPs were observed in response to CPF at different concentration ranges, thereby enabling good sensitivity and allowing a wide range of CPF concentrations to be detected. We observed that in conjunction with mild salt induction, CPF adsorbs to the surface of AuNPs at low concentrations, triggering them to further agglomerate, thereby allowing a progressively proportional SERS signal to be measured. However, at high CPF concentrations, an abundance of CPF molecules adsorb and cross-link the AuNPs, eventually resulting in complete and irreversible aggregation of the AuNPs. This process is unfavourable for SERS measurement, leading to an inverse SERS intensity at the higher pesticide concentration range. Subsequently, the method was applied to the detection of CPF present on cucumber peels to demonstrate the feasibility to real samples. Finally, the selectivity and reliability of the method were assessed using principal component analysis (PCA) modelling, which could successfully differentiate CPF from three other OPPs with similar chemical structures (profenofos, fenthion, and diazinon). Overall, the method reported herein shows great potential for the sensitive and specific detection of CPF across a wide range of concentrations.

2. Material and methods

2.1. Materials and reagents

Gold (III) chloride trihydrate ($HAuCl_4{\cdot}3H_2O$, 99.9%), sodium citrate tribasic dehydrate ($HOC(COONa)(CH_2\text{-}COONa)_2{\cdot}aq$), methanol ($CH_3OH$) ≥99.9%, rhodamine 6G (R6G), chlorpyrifos (CPF, $C_9H_{11}Cl_3NO_3PS$), profenofos ($C_{11}H_{15}BrClO_3PS$), fenthion ($C_{10}H_{15}O_3PS_2$), diazinon ($C_{12}H_{21}N_2O_3PS$), sodium chloride (NaCl), acetonitrile (ACN, C_2H_3N, ≥99.9%), magnesium sulphate ($MgSO_4$), n-propyl ethylenediamine (PSA), sodium acetate (CH_3COONa), acetic acid (CH_3COOH), 96-well flat-bottom microtitre plates and polyester foam-tipped sterile swabs were all purchased from Sigma Aldrich (UK). Organic cucumbers were purchased from a local supermarket (Tesco, UK).

2.2. Analysis instrumentation

Absorption spectroscopy measurements were performed using a Cary 60 UV–Vis spectrophotometer (Agilent Technologies, USA). Transmission electron microscopy (TEM) measurements were performed using a Joel JEM 1400 Plus model, operated at 200 kV (Thermo Fisher, Scientific, UK). Raman measurements were carried out using a DXR2 Raman microscope (Thermo Fisher Scientific, UK), and measurements were obtained using a 96-well microtitre plate, operated with an excitation laser light 785 nm with an exposure time of 5 s. A laser power of 25 mW was used unless otherwise stated.

2.3. Synthesis of colloidal AuNPs substrates

Spherical colloidal AuNPs were synthesised according to the previous method with slight adjustments (Logan, Lou-Franco, Elliott, & Cao, 2021). Specifically, 500 μL of $HAuCl_4$ (100 mM) was heated in 50 mL of dH_2O until boiling. Upon reaching reflux, 5 mL of sodium citrate (1%) was introduced quickly. Then, the colour transition from yellow to red wine marked the citrate-mediated reduction of gold ions. After 30 min of stirring, the colloidal AuNPs were cooled naturally to room temperature and stored at 4 °C for subsequent experiments. To obtain different concentrations of AuNPs, the prepared AuNPs were centrifuged at 6000 RCF for 60 min to eliminate excess supernatant. The concentration of AuNPs for subsequent experiments was calculated based on previous literature (Behzadi et al., 2015).

2.4. Analysis of CPF standard solution using SERS

Prior to analysis, a stock solution of CPF was prepared at a concentration of 1000 ppm in methanol and stored at 4 °C. Subsequent dilutions were prepared from the stock solution within the range 0.001 ppm (0.001 mg/kg) to 1000 ppm (1000 mg/kg) using 60% methanol (60:40 MeOH: dH_2O v/v). In a typical experiment, minor modifications were applied to a previously reported method (Logan et al., 2022). Firstly, the as-prepared AuNPs (275 μL) were mixed with CPF concentrations at 5 ppm and 50 ppm (55 μL). Thereafter, to observe the effect of salt induced agglomeration and aggregation, 3 M NaCl (3 μL) was added into the 5 ppm CPF and AuNP mixture, making a total volume of 333 μL in the microtitre plate. Moreover, to improve the sensitivity in the detection of CPF, optimization experiments were conducted with a fixed CPF concentration of 1 ppm (55 μL). Concentrations of AuNPs and NaCl were varied, maintaining consistent volumes, specified at 275 μL for AuNPs and 3 μL for NaCl. AuNPs concentrations were adjusted to 1, 5, 10, 15, and 20 M, and NaCl concentrations ranged between 1 and 6 M. Incubation times of 1, 2, 3, 5, 10, and 20 min were also optimized by monitoring their respective SERS intensities. Optimal conditions, determined by the highest SERS intensity for the detection of 1 ppm CPF, were identified as 15 M AuNPs, 4 M NaCl, and a 5-min incubation period. These parameters were subsequently utilized in further

experiments to detect CPF at various concentrations. All experiments were conducted in triplicates.

2.5. The analysis of CPF present in cucumber

Four extraction methods were examined in this study for the analysis of CPF residues from cucumber peels: (E1) Quick-Easy-Cheap-Effective-Rugged-Safe (QuEChERs) extraction (Mokhtari, Khosrowshahi, Farajzadeh, Nemati, & Afshar Mogaddam, 2022); (E2) acetonitrile (ACN)-sonication method; (E3) ACN-rinse method and (E4) a swabbing technique (detailed in Supplementary Information, Schematic 1 and Section 1). Prior to spiking with CPF, cucumber samples were cleaned thoroughly by rinsing in dH_2O, followed by air drying. Various concentrations of CPF standard solutions, ranging from 0.1 to 5 ppm, were then applied to approximately 1 cm^2 of the cucumber peel.

Confirmatory analysis of CPF was carried out using an Agilent 1290 Infinity II LC system coupled to a 6495B triple quadrupole mass spectrometer. Agilent MassHunter software was used for both data acquisition and processing. Chromatographic separation was performed using an Agilent Poreshell column, 30 × 2.1 mm, 2.7 µm maintained at 30 °C. The mobile phases comprised of methanol/water/acetic acid (10:89:1, v/v/v) and methanol/water/acetic acid (97:2:1, v/v/v) for mobile phases A and B, respectively, both containing 5 mM ammonium acetate. The elution was carried out following a gradient elution program as follows: 0 min 5% B, held for 0.5 min at 5% B, followed by 2.5 min 80% B, 4.5 min 95% B, 5.5 min 95% B, 6.5 min 5% B. Mobile phase flow rate was maintained at 0.4 mL/min, with sample injection volume set at 2.5 µL. The total runtime was 6.5 min. The mass spectrometry was operated in positive electrospray ionisation mode. The data acquisition was carried out in multiple reaction monitoring (MRM) mode, using the following transitions: 349.9 > 96.9 (Q) and 349.9 > 197.9 (q) with collision energies of 32 and 16 respectively.

2.6. Raman spectroscopy acquisition and chemometric analysis

Initially, the Raman spectra were acquired from 300 to 1800 cm^{-1}. All samples, including each pesticide and their mixtures with CPF, were prepared at a fixed concentration of 6 ppm to ensure uniform experimental conditions across all tests. Each sample was scanned in triplicates. The generated data was subsequently imported into SIMCA 14.1 chemometric software. After Pareto scaling, PCA was generated to identify the CPF, together with a mixture of 3 other pesticides. PCA compresses the original variables by projecting the data in a new space called principal components (PCs) in order to extract the major sources of variance. In this study, the performance of PCA model was evaluated by R^2 and Q^2. The R^2 was used to measure the fitting ability and the Q^2 was applied to assess the prediction accuracy of the model. R^2 and Q^2 equal to 1 indicate an effective model. This study analysed a total of 300 spectra from cucumber samples spiked with pesticides.

3. Results and discussion

3.1. Characterisation of AuNPs

Fig. 1 shows the characterisation of the synthesised AuNPs. The absorption spectrum in Fig. 1A, exhibits a unique localised surface plasmon resonance (LSPR) peak at 523 nm and the morphology of the as-prepared AuNPs was demonstrated via TEM. The image in Fig. 1B

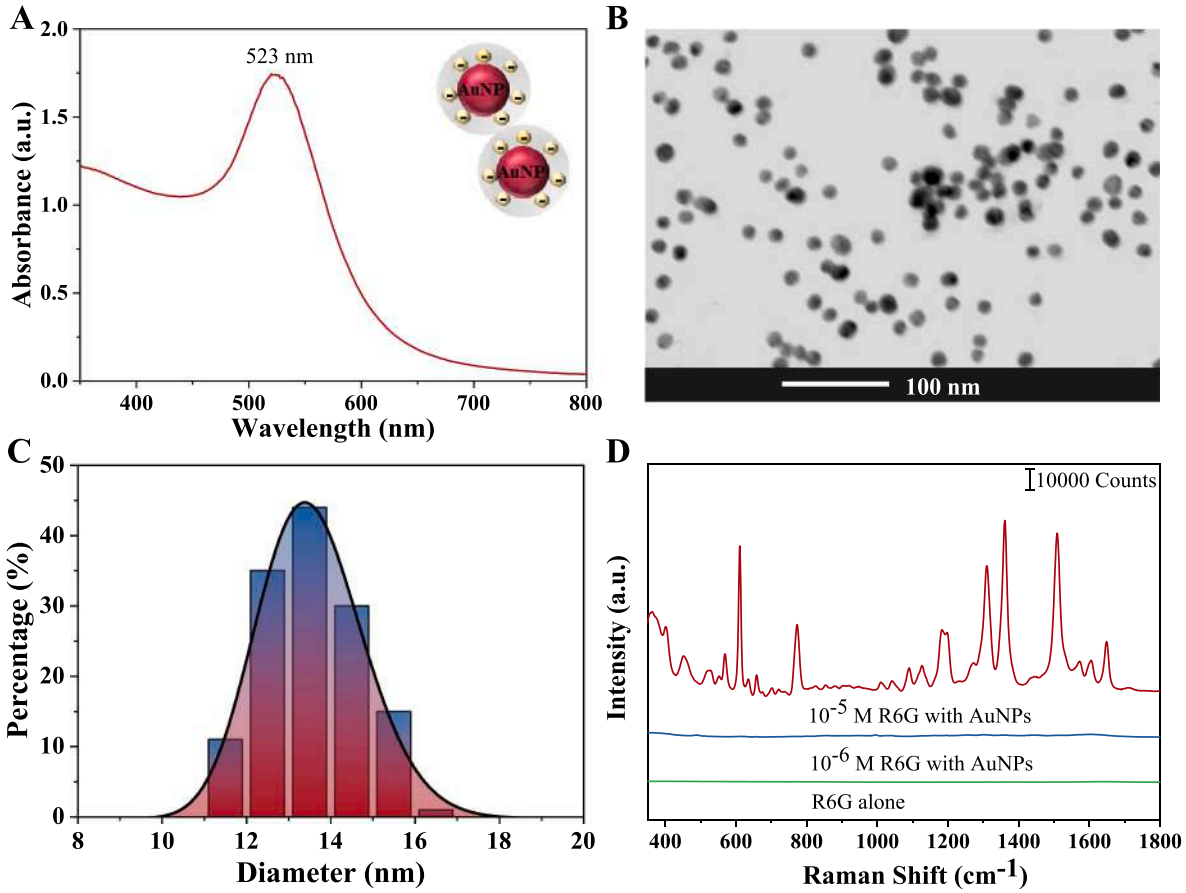

Fig. 1. Characterisation of AuNPs. (A) Absorption spectra of AuNPs indicating a maximum absorption peak (λ_{max}) at 523 nm. (B) Representative TEM images of AuNPs. (C) Histogram of diameter distribution indicating the average diameter of 13.8 ± 0.3 nm (calculated from 136 particles using Image J software). (D) SERS spectra of AuNPs (λ_{max} = 523 nm) with R6G (10^{-5} M and 10^{-6} M) and the Raman spectrum of R6G alone (10^{-5} M).

illustrates their spherical shape and uniformity in size, highlighting the average diameter of approximately 13.8 ± 0.3 nm (Fig. 1C). Thereafter, the SERS enhancement factor (EF) of the synthesised AuNPs was assessed using rhodamine 6G (R6G) as a probe molecule (Li et al., 2022; Li, Merkl, Sommertune, Thersleff, & Sotiriou, 2022). The main vibrational bands of R6G were observed at 1312 cm^{-1}, 1361 cm^{-1}, and 1510 cm^{-1}, corresponding to N—H bending, C—H bending, and C—N stretching, respectively (Fig. 1D and Table S2) (C. Zhang et al., 2021). Remarkably, the distinctive vibrational band at 1361 cm^{-1} was observed for concentrations as low as 10^{-5}M with an EF of 1.06 × 10^{4} was determined (see Supplementary Information Section 2 for the calculation of EF).

3.2. Synergistic effect of NaCl and CPF on the agglomeration and aggregation of AuNPs

It was evident that CPF can adsorb onto and cross-link AuNPs, with an increased concentration of CPF resulting in the agglomeration and aggregation of AuNPs. Fig. 2A illustrates the SERS spectrum of 10 ppm CPF in AuNP solution (red line) and the normal Raman spectrum of CPF powder (blue line). The spectra feature peaks corresponding to various functional groups, such as -C-H, -C-C-, -C-Cl-, -C-O-C-, P-O-C, Cl-ring, and -P=S-, with detailed assignments provided in Table S2 (Supplementary Information). Notably, the CPF-AuNPs spectrum exhibits obvious peak shift. For instance, the Cl-ring vibration shifted from 1239 cm^{-1} in the pure CPF powder to 1208 cm^{-1} in the CPF-AuNPs complex, and the P-O-C stretching is now observed at 412 cm^{-1} (Ma et al., 2020; Xu et al., 2017). This shift indicates the interaction between CPF molecules and AuNPs through either phosphate or chlorine groups rather than the pyridine ring, which exhibits minimal peak shift. Consequently, CPF is presumed to be oriented on the Au surface, with the antisymmetric stretching vibration of C=C being perpendicular to this surface (Xu et al., 2017). Accordingly, the most prominent peak at 1333 cm^{-1}, distinguished by its strong Raman signal, was identified for further investigation.

Further analysis reveals that increasing the concentration of CPF has

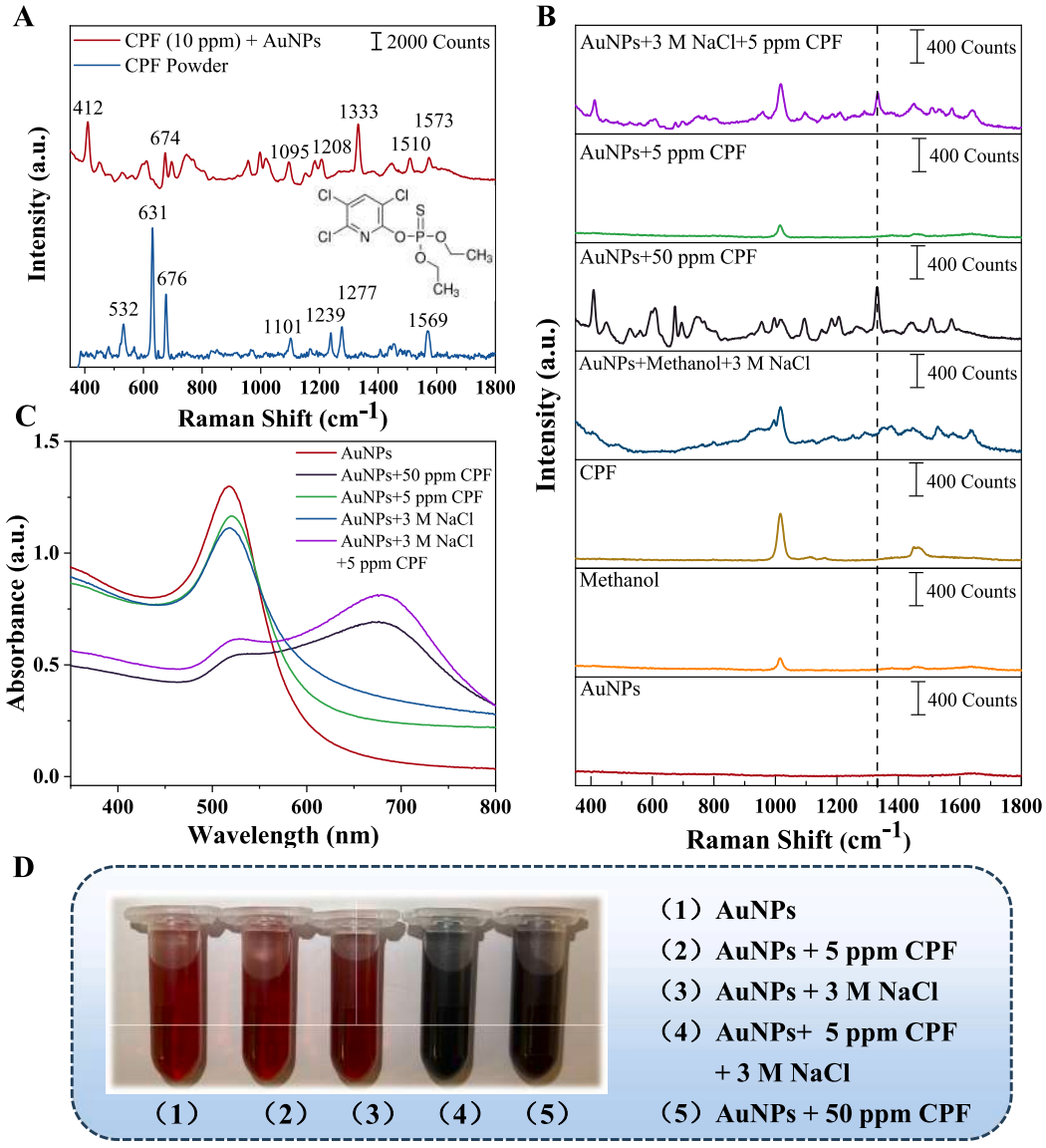

Fig. 2. Stability of colloidal AuNPs (λ_{max} = 523 nm) and corresponding SERS spectra in the presence of pesticides and NaCl. (A) Raman spectra of CPF powder (blue), a mixture of AuNPs with 10 ppm CPF (red) and the molecular structure of CPF. (B) SERS spectra for AuNPs, methanol, CPF in methanol, AuNPs with methanol and 3 M NaCl, AuNPs with CPF at 50 and 5 ppm and CPF in the presence of AuNPs and 3 μL of 3 M NaCl (starting from bottom to top). Representative (C) absorbance spectra and (D) colour images demonstrating the agglomeration/aggregation of AuNPs. (For interpretation of the references to colour in this figure legend, the reader is referred to the web version of this article.)

a significant impact on the behaviour of AuNPs. This phenomenon is primarily due to CPF's affinity for AuNPs, facilitated by specific phosphate and chlorine interactions that substantially disrupt the colloidal stability (Ngo, Trinh, & An, 2020). As a bifunctional crosslinker, CPF binds to adjacent nanoparticles, enhancing their agglomeration and leading to pronounced aggregation at higher concentrations. Additionally, CPF's partial positive charge counters the inherent negative charge of the AuNPs (Chadha et al., 2022), reducing the electrostatic repulsion between particles. This effect becomes more pronounced at CPF concentrations exceeding 5 ppm, leading to increased agglomeration and eventual aggregation in the range of 10–1000 ppm, as per the experimental conditions. The colorimetric changes and corresponding absorbance spectra post-agglomeration/aggregation with CPF are demonstrated in Fig. S2.

Upon observing that CPF concentrations below 5 ppm were insufficient to induce notable agglomeration and aggregation of AuNPs, the study extended to examine the combined effects of NaCl and CPF on AuNPs aggregation. As shown in Fig. 2B, the SERS signal of CPF could not be observed at 5 ppm of CPF (green line), and it was only obtained when the concentration increased to 50 ppm (black line). Furthermore, the addition of NaCl resulted in a notable red shift in absorbance, as depicted in Fig. 2C (purple line), indicating enhanced nanoparticle aggregation. This aggregation, stimulated by NaCl in conjunction with CPF, effectively aligned the LSPR wavelength of the AuNPs closer to the laser excitation wavelength of 785 nm (Logan et al., 2021). This alignment explains the observed increase in Raman enhancement, as the closer proximity of the LSPR wavelength to 785 nm optimizes the electromagnetic field enhancement, particularly demonstrated in Fig. 2B (purple line).

In fact, we further examined particle agglomeration and aggregation, as demonstrated in Fig. 2C and D, to observe the absorbance behaviour and colorimetric changes under the influence of CPF and NaCl in AuNP solutions, respectively. At a CPF concentration of 5 ppm, the addition of NaCl could elicit a synergistic effect, significantly enhancing AuNPs' agglomeration and aggregation, as indicated by the significant red shift (Fig. 2C, purple line) and a colour change from wine red to dark blue (Fig. 2D). This is attributed to NaCl in displacing the citrate ions on the surface of AuNPs, decreasing the negative charge of the nanoparticles. Subsequently, the addition of NaCl leads to an increase in the ionic strength of the solution, which reduces the electrostatic repulsion between nanoparticles (Bickel et al., 2016; Khrushchev et al., 2022), thereby achieving effective aggregation with fewer CPF molecules. A microscopic view representing agglomeration and aggregation can be seen through the TEM images (Fig. S3, Supplementary Information). This effect is reflected by the absorbance ratio of A523/A680: as agglomeration progresses to aggregation, the plasmon resonance undergoes a red shift, resulting in the emergence of a second peak at 680 nm. This transition is indicative of the AuNPs moving from a loosely clustered state (agglomeration) to a more structured and stable group (aggregation) (Zook, Maccuspie, Locascio, Halter, & Elliott, 2011), especially in the presence of NaCl, which facilitates the detection of CPF using SERS (Fig. 2B, purple line). As shown in Table S3, for AuNPs, the A523/A680 value was 16.00, representing the monodispersed AuNP solution, which decreases gradually to 4.60, 3.06, 0.75, and 0.78 after the addition of 5 ppm CPF, 3 M NaCl, 5 ppm CPF with 3 M NaCl, and 50 ppm CPF respectively. These results signify initial agglomeration eventually leading to aggregation with the emergence of another peak at 680 nm. These results unequivocally confirm the critical role of NaCl in assisting the sensitive detection of CPF at trace levels using SERS.

3.3. Dynamic range of SERS-based detection of CPF

The optimized experimental parameters were utilized to assess the capability of the SERS sensor for detecting CPF standard solutions. Based on these results, a concentration of 15 M of AuNPs, 4 M of NaCl, and a 5-min incubation period were found to provide the highest SERS signals and therefore were utilized to detect CPF at various concentrations (Fig. S4, Supplementary Information). Fig. 3A schematically illustrates the dispersion, agglomeration and aggregation influenced by increasing CPF concentrations. Notably, the peak at 1333 cm^{-1} was identified as a characteristic peak of CPF due to its significant SERS intensity variation with different concentrations, as shown in Fig. 3B. At lower concentrations (0.001 to 1 ppm, Fig. 3C), CPF adsorbs on the surface of AuNPs, promoting a weaker form of agglomeration, which further strengthens with the addition of NaCl, thereby allowing a proportional SERS signal to be measured. As a result, a linear correlation with regression equation as $y = 206.19\times + 24.229$ with a correlation coefficient value for R^2 as 0.97 can be observed, indicating high precision when exploiting the Raman signal intensity at 1333 cm^{-1} (Fig. 3D). The limit of detection (LOD) and the limit of quantification (LOQ) are calculated using the IUPAC definition and formulas 3S/M and 10S/M, respectively, were S is the standard deviation of ten measurements of the blank solution, and M is the slope of the calibration curve (Long & Winefordner, 1983). The results confirmed a linear relationship with the LOD and LOQ value of 0.009 ppm and 0.031 ppm.

In contrast, at higher concentrations of CPF from 1 to 1000 ppm (Fig. 3E), an abundance of CPF molecules continue to adsorb and crosslink the AuNPs gradually, eventually resulting in their stronger form of aggregation. This phenomenon leads to a disruption of the hotspot sites, significantly diminishing the number of available sites for SERS enhancement, thereby adversely affecting the SERS measurements. This phenomenon results in inverse sensitivity with an exponential regression equation as $y = 391.07\times^{-0.715}$, with $R^2 = 0.95$. Within this range, an inverse linear response curve can be seen from 1 to 5 ppm ($y = -46.419\times + 355.84$, $R^2 = 0.93$), in which the inverse limit of detection (iLOD) is defined as the lowest concentration at which the inverse sensitivity response began to manifest (Pallares, Thanh, & Su, 2018), i.e. 1 ppm (Fig. 3E). It should be noted that the selection of the aggregation agent, alongside the concentration of AuNPs and the duration of incubation required for optimal signal generation, may exhibit considerable variability due to differential rates of agglomeration and aggregation. The experimental conditions in this experiment have been extensively optimized to assure the consistency of experimental parameters. As a result, the agglomeration and aggregation of AuNPs enable the detection of CPF across a wide concentration range (10^{-3} to 5 ppm) with two distinct linear detection curves: (i) 0.001 to 1 ppm and (ii) an inverse linear response curve from 1 to 5 ppm. This facilitates sensitive CPF detection and highlights the correlation between CPF concentration and AuNPs' agglomeration and aggregation states.

The non-linear, bell-shaped dynamic response witnessed when studying the full dynamic range of CPF concentrations poses a challenge in terms of quantification, as one Raman intensity value may represent two concentrations, as depicted in Fig. 3C. However, this issue can be addressed when combined with the colorimetric response of AuNPs under different CPF concentrations. As demonstrated in Fig. 4A, the solution progressively transitions in colour from red to dark purple, subsequently to dark blue, and finally to lighter grey with increasing CPF concentrations (0–1000 ppm), attributing to the gradual transition from agglomeration to aggregation of AuNP solutions. Alternatively, this can further be achieved by assessing the optical absorption behaviour based on collective electronic oscillations of the nanoparticles. As shown in Fig. 4B, with increasing CPF concentration, the peak around 523 nm shifts to longer wavelengths, indicating the growth of particle clusters and the broadening of the peak (Chadha, Das, Kapoor, & Maiti, 2021). Notably, in Fig. S5 (Supplementary Information), the absorbance ratio A523/A680 changes from 2.81 (for 0 ppm CPF) to 0.39 (for 100 ppm CPF), implying the presence of larger aggregated clusters of nanoparticles. Therefore, by combining the colorimetric and plasmonic responses, this could provide valuable insights into the agglomeration and aggregation phenomena, enhancing the accuracy of CPF quantification.

In addition, unsupervised PCA model could be used to effectively differentiate various concentrations of the CPF in this case. PCA discerns

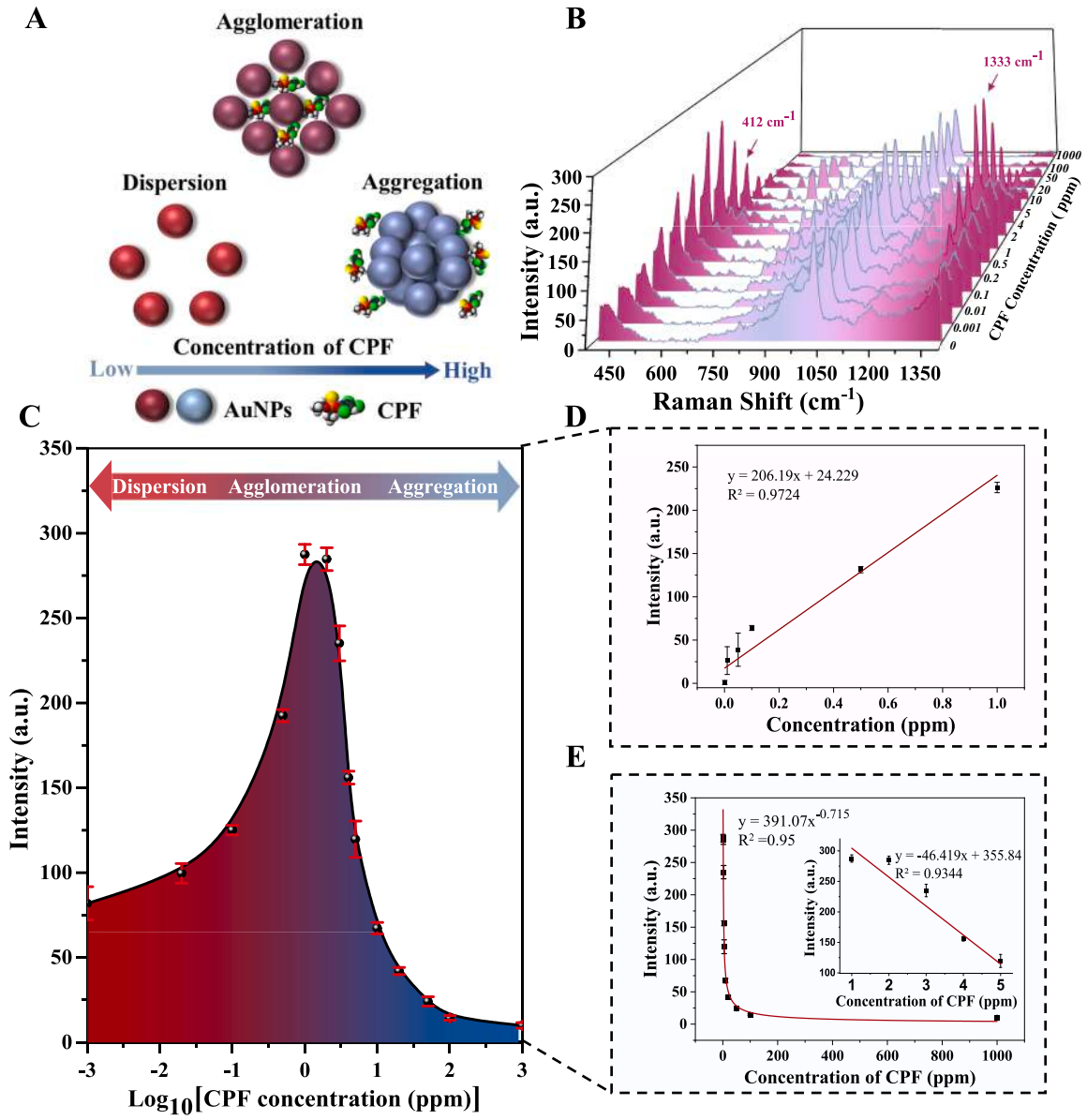

Fig. 3. SERS-based detection of CPF. (A) A schematic representation of the stability states of AuNPs under the effect of increasing concentrations of CPF. (B) SERS spectra of solutions containing 275 μL of 15 M AuNPs, 3 μL of 4 M NaCl, and 55 μL of CPF at various concentrations (0–1000 ppm). (C) Dynamic range analysis demonstrating SERS intensity at the diagnostic peak of 1333 cm^{-1} versus CPF concentrations, exhibiting non-linear concentration responses. (D) At the lower concentration range of CPF (i.e. 0.001 to 1 ppm), the SERS intensity was proportional to the CPF concentrations. However, at the higher concentration range (i.e. 1 to 1000 ppm), an inverse SERS signal to the concentration was observed (E).

the variations in the SERS spectra corresponding to CPF across a broad concentration range. Based on the SERS measurements of the 70 samples, the PCA model was carried out and the corresponding score plot has been shown in Fig. 4C. Specifically, the lower concentrations (0.01 ppm, 0.1 ppm, 1 ppm) situated on the left side and the higher concentrations (5 ppm, 10 ppm, 50 ppm, 100 ppm, 1000 ppm) located on the right side of the PC1 axis, which accounted for 77% of the total variance. The results not only effectively distinguish between low concentrations (< 5 ppm) and high (5–1000 ppm), but also exhibit tight clustering and distinct separation across various concentration groups. This approach provides an efficient way for the sample detection of unknown concentrations.

Overall, the developed method enables the detection of CPF across various concentration ranges. In the low concentration range (0.001–1 ppm), the SERS detection signal shows a linear relationship with the concentration of the target analyte, allowing CPF to be detected as low as 0.009 ppm. Conversely, at higher concentrations (1–1000 ppm), an inverse response occurs, with an inverse linear regression observed from 1 to 5 ppm and an iLOD of 1 ppm. When dealing with CPF samples of uncertain concentrations, distinguishing between these phenomena is possible based on employing a bell-shaped curve coupled with their colorimetric response of AuNP solutions, absorbance spectra, and the PCA as presented above. The combined dose response analyses with PCA could allow the reliable detection of CPF in samples with unknown concentrations.

3.4. The detection of CPF on cucumber surface

Cucumber (*Cucumis sativus*), belonging to the gourd family, is a globally consumed vegetable (Feng et al., 2021). Its cultivation often requires substantial pesticide use due to high demand and susceptibility to insect attacks (Khoshnam, Ziaee, Daei, Mahdavi, & Mousavi

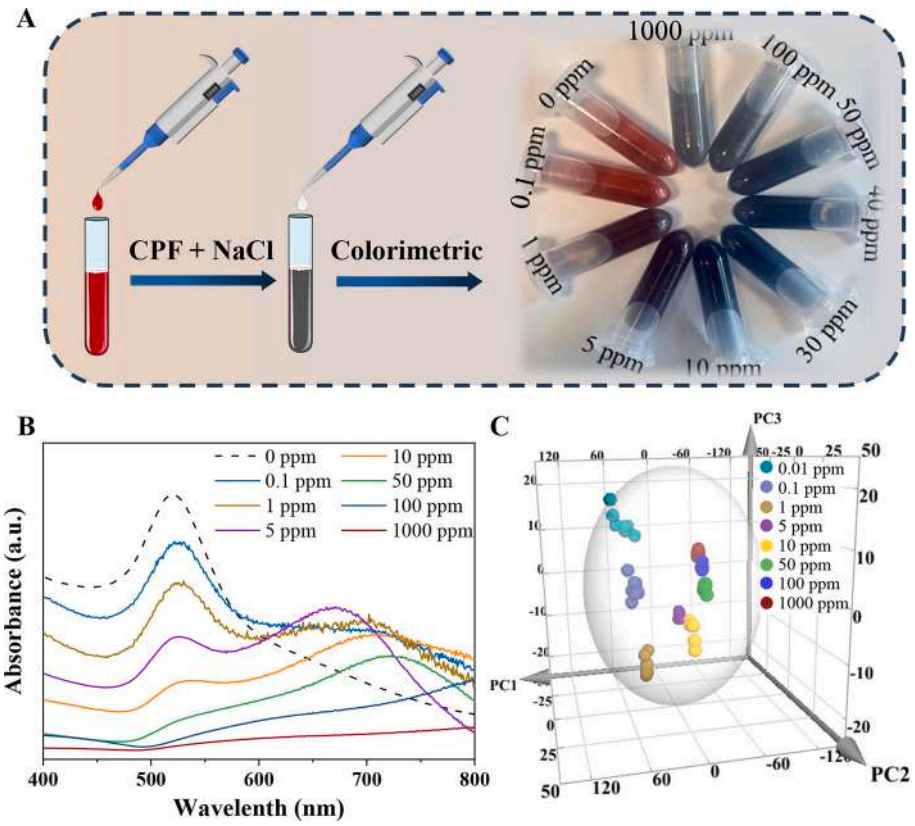

Fig. 4. Analysis of CPF standard solutions: 55 μL of CPF at various concentrations (0–1000 ppm) interacted with 275 μL of 15 M AuNPs and 3 μL of 4 M NaCl. (A) Colour image of the mixed solutions, (B) absorption spectra, and (C) PCA analysis of CPF at various concentrations.

Khaneghah, 2022). This study evaluated the effectiveness of SERS for the analysis of cucumbers contaminated with pesticides, which often reside on the surface. Four extraction methods for CPF recovery from cucumber peels were assessed: (E1) QuEChERs extraction, (E2) ACN-sonication method, (E3) ACN-rinse method and (E4) a swabbing technique. A comparative analysis of recovery efficacy revealed that E1 and E2 were ineffective in recovering CPF from cucumber peels for Raman analysis (Fig. S6 A). This is potentially attributable to the concurrence of

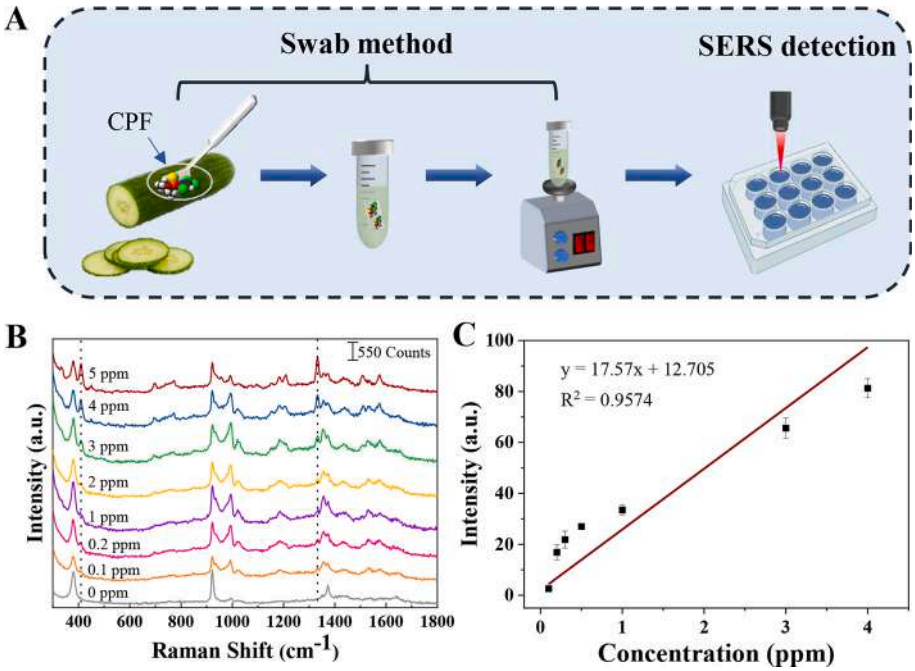

Fig. 5. CPF residues at different concentrations were detected on the cucumber surface using SERS. (A) Schematic illustration of swab method employed, and corresponding SERS detection of pesticides released from swab. (B) The SERS spectra of CPF obtained after swabbing from spiked cucumbers. (C) Linear relationship between increasing SERS intensity and CPF concentration swabbing from cucumbers.

chlorophyll within the recovered CPF samples. Consequently, fluorescence from chlorophyll significantly interfered with the weak Raman signal of CPF. However, E3 and E4 could successfully extract CPF, with the swab method (E4) yielding stronger SERS signals (Fig. S6 A), which may be due to enhanced CPF removal via frictional forces. Thereafter, to optimize the swab method, four solvents (acetone, acetonitrile, methanol, and ethanol) were employed and compared subsequently (Fig. S6 B), resulting in acetonitrile being most effective, aligning with prior findings of CPF's high solubility in acetonitrile (Shabbir, Singh, Maiti, & Saha, 2021). Consequently, the swab method with acetonitrile, coupled with SERS, was selected for subsequent CPF analysis on cucumber surfaces.

The schematic in Fig. 5A shows the residues of CPF on the surface of the cucumber peels as detected using SERS combined with the modified surface swab method. Cucumber peels were exposed to CPF concentrations ranging from 0.1 to 5 ppm. The SERS spectra revealed distinct CPF vibrational bands on the peels, which intensified with increasing CPF levels (Fig. 5B). The characteristic peak at CPF at 1333 cm^{-1} shows the calibration curve represented by the fitted linear model, $y = 17.57\times + 12.705$, and exhibits a high degree of accuracy ($R^2 = 0.96$) as shown in Fig. 5C. Moreover, the LOD was calculated to be 0.11 ppm and LOQ as 0.37 ppm on the cucumber surface. To assess the reproducibility of the method, the relative standard deviation (RSD) was evaluated at a low concentration of 1 ppm. This was accomplished by recording Raman intensities at 1333 cm^{-1} for 20 cucumber peel samples, yielding an RSD of 11.83% (Fig. S7, Supplementary Information). Furthermore, LC-MS/MS analysis using an Agilent 6545B QqQ mass spectrometer was conducted to further verify these results, as shown in Fig. S8. The cucumber samples were first tested unspiked to confirm cucumbers were 'negative' for CPF. Subsequent LC-MS/MS analysis of cucumber samples spiked with CPF at the LOD of 0.11 ppm for the analytical platform (SERS) and carried out the same extraction protocol for CPF. The clean and spiked cucumber samples were carried out in quadruplicate and analysed using LC-MS/MS, with the chromatographic traces confirming the presence of CPF. The ion ratio (q/Q) and retention time (RT) of CPF in the spiked sample matched that of the CPF solvent standard, confirming its presence. Thus, the application of a swab technique for collecting CPF residues from cucumber surfaces, followed by detection using SERS, demonstrates good accuracy. This method is further validated by confirmatory LC-MS/MS analyses, ensuring a comprehensive and

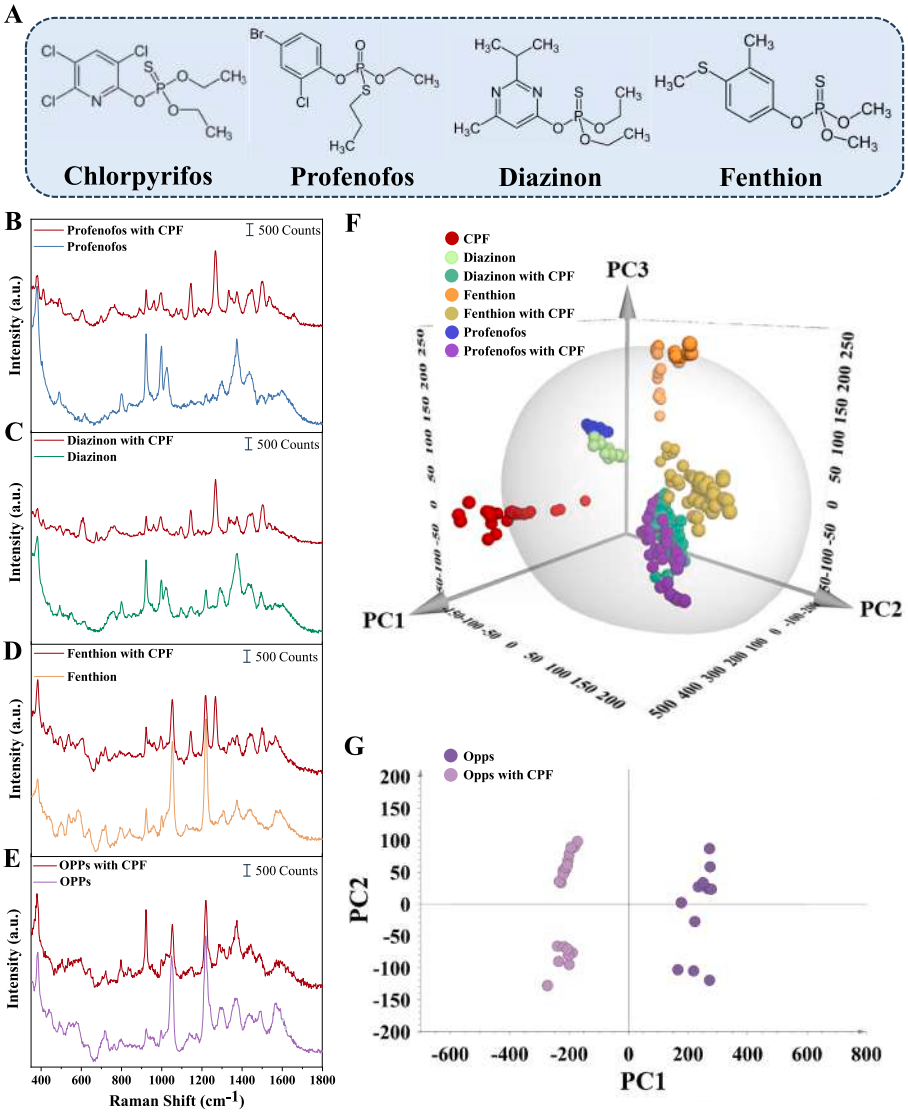

Fig. 6. Identification of CPF in the presence of other OPPs on cucumber samples to assess the method's selectivity and reliability. (A) The chemical structures of chlorpyrifos, profenofos, diazinon and fenthion. (B—D) SERS spectra of profenofos, diazinon and fenthion and their mixtures with CPF. (E) SERS spectra of all three pesticides together (profenofos, diazinon and fenthion) and then mixed with CPF. (F) The three-dimensional PCA plot showing the separation of the individual pesticide classes and their mixtures with CPF. (G) A two-dimensional PCA plot showing the separation of all three pesticides together and then mixed with CPF.

reliable evaluation of pesticide residue detection on cucumbers.

3.5. Chemometric analysis for the identification of CPF

In agricultural production, the synergistic application of multiple OPPs is common to control pests effectively, invariably leading to the accumulation of OPPs residues in agricultural produce (Li, Wang, et al., 2022). Fig. 6A demonstrates the chemical structure of chlorpyrifos, profenofos, diazinon, and fenthion respectively, which are common OPPs, and their structural similarities pose significant challenges in spectral discrimination using SERS techniques. Additionally, Fig. S8 distinctly presents the SERS spectra for this set of OPPs and shows that several bands are closely aligned, implying a degree of spectral similarity which could potentially lead to analytical ambiguities, i.e. a false positive response. Furthermore, adding to the complexity, Fig. 6B-E showcases the Raman spectra of these pesticides, all at 6 ppm (including their respective mixtures with CPF), captured using the swab method on cucumber surfaces. Although Raman spectroscopy is known for its ability to provide distinct spectral fingerprints for different pesticides, any intense spectral features significantly hinder the precise identification of the target pesticide. This may lead to analytical inaccuracies, such as misinterpretations, or omissions (false negative). Therefore, it is necessary to employ advanced analytical techniques, including comprehensive chemometric analyses, to accurately differentiate and quantify individual pesticide residues within complex agricultural matrices.

To clearly identify CPF within a mixture, PCA was utilized further in the selectivity study. PCA is an unsupervised pattern recognition technique, aims to visualize the natural clustering and variability within the samples by using dimensionality reduction and linear feature extraction approaches (Hong et al., 2023). The PCA score plot has been shown in Fig. 6F, demonstrating a clear separation among profenofos, fenthion, and diazinon, their mixture with CPF and CPF alone. The first three PCs cumulatively explained 87.3% of the total variance, with PC1 at 47.3%, PC2 at 23.2%, and PC3 at 16.8%. An R^2 value of 0.99 confirms the model's robust fit, while a Q^2 of 0.98 underscores its excellent predictive quality. CPF exhibits distinct grouping and separation from profenofos, fenthion, and diazinon, which are structurally similar OPPs, as indicated by the red coloured cluster. Clear separation can also be observed when CPF was mixed with profenofos, fenthion, and diazinon, respectively, compared to these pesticides alone. In addition, the study demonstrated the CPF can be distinctly recognized even when all three OPPs are co-present together (Fig. 6G). The projection plot of the first two PCs cumulatively accounted for 95.8% of the total variation with PC1 explaining 87.6% and PC2 explaining 8.2%. The R^2 and Q^2 values of the PCA model were 0.99 and 0.98, respectively, highlighting the model's robust predictive capability to detect CPF within a complex mixture. Overall, the results indicate that Raman spectroscopy combined with PCA showed strong potential for the accurate identification of CPF from multiple pesticides.

4. Conclusions

This study presents a detailed insight into the agglomeration and aggregation of AuNPs for the detection of CPF by means of SERS. Upon combination with salt induction, the SERS signal was not always proportional to the concentrations of the CPF target analyte. In fact, a linear relationship was observed at low concentrations of CPF ranging from 0.001 to 1 ppm, with a LOD of 0.009 ppm. However, at CPF concentrations higher than 1 ppm, the SERS signal exhibited an inverse proportionality to the concentration of the target analyte. For samples with uncertain CPF levels, we found that the combined analysis of the colorimetric response of AuNP solutions, their absorbance spectra, and PCA could facilitate the reliable detection of CPF across a wide concentration range. In real sample testing, a straightforward technique for CPF recovery from cucumbers through swabbing using ACN demonstrated high reproducibility, with an LOD of 0.11 ppm and an RSD of 11.83%. This method could allow for a customized detection approach, where desirable CPF concentrations to be detected can be tuned. The application of chemometrics further enhances selectivity, aiding in the accurate identification of CPF among similar pesticides not only in cucumber samples but also in various other fruits and food matrices.

CRediT authorship contribution statement

Xiaotong Liu: Writing – review & editing, Writing – original draft, Methodology, Investigation, Formal analysis, Data curation, Conceptualization. **Udit Pant:** Writing – review & editing, Formal analysis. **Natasha Logan:** Writing – review & editing, Writing – original draft, Formal analysis. **Qiqi He:** Writing – review & editing, Methodology, Formal analysis, Data curation. **Brett Greer:** Writing – review & editing, Methodology, Formal analysis, Data curation. **Christopher T. Elliott:** Writing – review & editing, Supervision, Resources, Formal analysis, Conceptualization. **Cuong Cao:** Writing – review & editing, Writing – original draft, Supervision, Resources, Methodology, Funding acquisition, Formal analysis, Conceptualization.

Declaration of competing interest

The authors declare that they have no known competing financial interests or personal relationships that could have appeared to influence the work reported in this paper.

Data availability

Data will be made available on request.

Acknowledgements

The authors X.L., N.L., C.E., and C.C. acknowledge the funding provided as part of the Horizon Europe Framework Programme Horizon-CL6-2021-FARM2FORK01 grant agreement under Project No. 101059813 (HOLiFOOD).

Appendix A. Supplementary data

Supplementary data to this article can be found online at https://doi.org/10.1016/j.foodchem.2024.139944.

References

Behzadi, S., Ghasemi, F., Ghalkhani, M., Ashkarran, A. A., Akbari, S. M., Pakpour, S., & Mahmoudi, M. (2015). Determination of nanoparticles using UV-vis spectra. *Nanoscale, 7*(12), 5134–5139. https://doi.org/10.1039/c4nr00580e

Bickel, F., Herold, E. M., Signes, A., Romeijn, S., Jiskoot, W., & Kiefer, H. (2016). Reversible NaCl-induced aggregation of a monoclonal antibody at low pH: Characterization of aggregates and factors affecting aggregation. *European Journal of Pharmaceutics and Biopharmaceutics, 107*, 310–320. https://doi.org/10.1016/j.ejpb.2016.07.020

Chadha, R., Das, A., Kapoor, S., & Maiti, N. (2021). Surface-induced dimerization of 2-thiazoline-2-thiol on silver and gold nanoparticles: A surface enhanced Raman scattering (SERS) and density functional theoretical (DFT) study. Journal of Molecular Liquids, 322, Articles 114536. Doi: https://doi.org/10.1016/j.molliq.2020.114536.

Chadha, R., Das, A., Lobo, J., Meenu, V. O., Paul, A., Ballal, A., & Maiti, N. (2022). γ-Cyclodextrin capped silver and gold nanoparticles as colorimetric and Raman sensor for detecting traces of pesticide “Chlorpyrifos” in fruits and vegetables. Colloids and Surfaces A: Physicochemical and Engineering Aspects, 641, Articles 128558. Doi: https://doi.org/10.1016/j.colsurfa.2022.128558.

Chan, M. Y., Leng, W., & Vikesland, P. J. (2018). Surface-enhanced Raman spectroscopy characterization of salt-induced aggregation of gold nanoparticles. *ChemPhysChem, 19*(1), 24–28. https://doi.org/10.1002/cphc.201700798

Chang, H., Kang, H., Ko, E., Jun, B.-H., Lee, H.-Y., Lee, Y.-S., & Jeong, D. H. (2016). PSA detection with Femtomolar sensitivity and a broad dynamic range using SERS Nanoprobes and an area-scanning method. *ACS Sensors, 1*(6), 645–649. https://doi.org/10.1021/acssensors.6b00053

Cholula-Diaz, J. L., Lomeli-Marroquin, D., Pramanick, B., Nieto-Arguello, A., Cantu-Castillo, L. A., & Hwang, H. (2018). Synthesis of colloidal silver nanoparticle clusters and their application in ascorbic acid detection by SERS. *Colloids Surfaces B Biointerfaces, 163*, 329–335. https://doi.org/10.1016/j.colsurfb.2017.12.051

EFSA. (2019). Updated statement on the available outcomes of the human health assessment in the context of the pesticides peer review of the active substance chlorpyrifos-methyl. *EFSA Journal, 17*(11). https://doi.org/10.2903/j.efsa.2019.5908

Evenson, R. E., & Gollin, D. (2003). Assessing the impact of the green revolution, 1960 to 2000. *Science, 300*(5620), 758–762. https://doi.org/10.1126/science.1078710

Feng, X. X., Pan, L. X., Jing, J., Zhang, J. C., Zhuang, M., Zhang, Y., & Zhang, H. Y. (2021). Dynamics and risk assessment of pesticides in cucumber through field experiments and model simulation. *Science of the Total Environment, 773*, Article 145615. https://doi.org/10.1016/j.scitotenv.2021.145615

Hong, Y., Birse, N., Quinn, B., Li, Y., Jia, W., McCarron, P., & Elliott, C. T. (2023). Data fusion and multivariate analysis for food authenticity analysis. Nature. *Communications, 14*(1), Article 3309. https://doi.org/10.1038/s41467-023-38382-z

Kang, M., Kim, H., Oleiki, E., Koo, Y., Lee, H., Joo, H., & Park, K. D. (2022). Conformational heterogeneity of molecules physisorbed on a gold surface at room temperature. Nature. *Communications, 13*(1), Article 4133. https://doi.org/10.1038/s41467-022-31576-x

Khoshnam, F., Ziaee, M., Daei, M., Mahdavi, V., & Mousavi Khaneghah, A. (2022). Investigation and probabilistic health risk assessment of pesticide residues in cucumber, tomato, and okra fruits from Khuzestan, Iran. *Environmental Science and Pollution Research, 29*(17), 25953–25964. https://doi.org/10.1007/s11356-022-19041-0

Khrushchev, A. Y., Akmaev, E. R., Gulyaeva, A. Y., Zavialov, A. V., Sidorenko, A. I., Bondarenko, V. O., & Lvovskiy, A. I. (2022). Ion-induced agglomeration of ag NPs for quantitative determination of trace malachite green in natural water by SERS. *Vibrational Spectroscopy, 120*. https://doi.org/10.1016/j.vibspec.2022.103360

Langer, J., Jimenez de Aberasturi, D., Aizpurua, J., Alvarez-Puebla, R. A., Auguie, B., Baumberg, J. J., & Liz-Marzan, L. M. (2020). Present and future of surface-enhanced Raman scattering. *ACS Nano, 14*(1), 28–117. https://doi.org/10.1021/acsnano.9b04224

Leskovac, A., & Petrović, S. (2023). Pesticide use and degradation strategies: Food safety, challenges and perspectives. *Foods, 12*(14), Article 2709. https://doi.org/10.3390/foods12142709

Li, H., Merkl, P., Sommertune, J., Thersleff, T., & Sotiriou, G. A. (2022). SERS hotspot engineering by aerosol self-assembly of Plasmonic ag nanoaggregates with tunable Interparticle distance. Advanced. *Science, 9*(22), Article 2201133. https://doi.org/10.1002/advs.202201133

Li, R., Wang, Z., Zhang, Z., Sun, X., Hu, Y., Wang, H., & Chen, X. (2022). Deep learning-based multicapturer SERS platform on Plasmonic Nanocube Metasurfaces for multiplex detection of organophosphorus pesticides in environmental water. *Analytical Chemistry, 94*(46), 16006–16014. https://doi.org/10.1021/acs.analchem.2c02973

Logan, N., Haughey, S. A., Liu, L., Burns, D. T., Quinn, B., Cao, C., & Elliott, C. T. (2022). Handheld SERS coupled with QuEChERs for the sensitive analysis of multiple pesticides in basmati rice. npj Science of Food, 6(1), Article 3 Doi: https://doi.org/10.1038/s41538-021-00117-z.

Logan, N., Lou-Franco, J., Elliott, C., & Cao, C. (2021). Catalytic gold nanostars for SERS-based detection of mercury ions (Hg2+) with inverse sensitivity. *Environmental Science: Nano, 8*(9), 2718–2730. https://doi.org/10.1039/d1en00548k

Long, G. L., & Winefordner, J. D. (1983). Limit of detection a closer look at the IUPAC definition. *Analytical Chemistry, 55*(07), 712A–724A. https://doi.org/10.1021/ac00258a724

Lu, Y., Tan, Y., Xiao, Y., Li, Z., Sheng, E., & Dai, Z. (2021). A silver@gold nanoparticle tetrahedron biosensor for multiple pesticides detection based on surface-enhanced Raman scattering. *Talanta, 234*, Article 122585. https://doi.org/10.1016/j.talanta.2021.122585

Ma, P., Wang, L., Xu, L., Li, J., Zhang, X., & Chen, H. (2020). Rapid quantitative determination of chlorpyrifos pesticide residues in tomatoes by surface-enhanced Raman spectroscopy. *European Food Research and Technology, 246*(1), 239–251. https://doi.org/10.1007/s00217-019-03408-8

Malik, P., Sarker, D., Kumar, D., Schwartzkopf, M., Srivastava, P., & Ghosh, S. (2023). Tuning LSPR of thermal spike-induced shape-engineered au nanoparticles embedded in Si(3)N(4) thin-film matrix for SERS applications. *ACS Applied Materials & Interfaces, 15*(38), 45426–45440. https://doi.org/10.1021/acsami.3c08834

Mokhtari, S., Khosrowshahi, E. M., Farajzadeh, M. A., Nemati, M., & Afshar Mogaddam, M. R. (2022). A modified quick-easy-cheap-effective-rugged-and-safe method involving carbon nano-onions-based dispersive solid-phase extraction and dispersive liquid–liquid microextraction for pesticides from grapes. *Journal of Separation Science, 45*(18), 3582–3593. https://doi.org/10.1002/jssc.202200124

Ngo, T. C., Trinh, Q. T., Thi Thai An, N., Tri, N. N., Trung, N. T., Truong, D. H., . . . Dao, D. Q. (2020). SERS spectra of the pesticide Chlorpyrifos adsorbed on silver Nanosurface: The Ag20 cluster model. The Journal of Physical Chemistry C, 124(39), 21702–21716. Doi: https://doi.org/10.1021/acs.jpcc.0c06078.

Ore, O. T., Adeola, A. O., Bayode, A. A., Adedipe, D. T., & Nomngongo, P. N. (2023). Organophosphate pesticide residues in environmental and biological matrices: Occurrence, distribution and potential remedial approaches. *Environmental Chemistry and Ecotoxicology, 5*, 9–23. https://doi.org/10.1016/j.enceco.2022.10.004

Pallares, R. M., Thanh, N. T. K., & Su, X. (2018). Tunable plasmonic colorimetric assay with inverse sensitivity for extracellular DNA quantification. *Chemical Communications, 54*(80), 11260–11263. https://doi.org/10.1039/c8cc05465g

Park, B., Dang, T. V., Yoo, J., Tran, T. D., Ghoreishian, S. M., Lee, G. H., & Huh, Y. S. (2022). Silver nanoparticle-coated polydopamine-copper hybrid nanoflowers as ultrasensitive surface-enhanced Raman spectroscopy probes for detecting thiol-containing molecules. *Sensors and Actuators B: Chemical, 369*, Article 132246. https://doi.org/10.1016/j.snb.2022.132246

Parliament, U. (2021). Pesticides and health: UK Parliament POST. Available at: https://researchbriefings.files.parliament.uk/documents/POST-PB-0043/POST-PB-0043.pdf.

Schreinemachers, P., Afari-Sefa, V., Heng, C. H., Dung, P. T. M., Praneetvatakul, S., & Srinivasan, R. (2015). Safe and sustainable crop protection in Southeast Asia: Status, challenges and policy options. *Environmental Science & Policy, 54*, 357–366. https://doi.org/10.1016/j.envsci.2015.07.017

Shabbir, M., Singh, M., Maiti, S., & Saha, S. K. (2021). Organophosphate pesticide (Chlorpyrifos): Environmental menace; study reveals genotoxicity on plant and animal cells. Environmental. *Challenges, 5*, Article 100313. https://doi.org/10.1016/j.envc.2021.100313

Tabibi, A., & Jafari, M. T. (2022). High efficient solid-phase microextraction based on a covalent organic framework for determination of trifluralin and chlorpyrifos in water and food samples by GC-CD-IMS. *Food Chemistry, 373*(2022), Article 131527. https://doi.org/10.1016/j.foodchem.2021.131527

Wang, K., Yue, Z., Fang, X., Lin, H., Wang, L., Cao, L., & Ju, L. (2023). SERS detection of thiram using polyacrylamide hydrogel-enclosed gold nanoparticle aggregates. *Science of the Total Environment, 856*, Article 159108. https://doi.org/10.1016/j.scitotenv.2022.159108

Weerathunge, P., Behera, B. K., Zihara, S., Singh, M., Prasad, S. N., Hashmi, S., & Ramanathan, R. (2019). Dynamic interactions between peroxidase-mimic silver NanoZymes and chlorpyrifos-specific aptamers enable highly-specific pesticide sensing in river water. *Analytica Chimica Acta, 1083*, 157–165. https://doi.org/10.1016/j.aca.2019.07.066

Xiong, Y., Huang, J., Wu, R., Geng, X., Zuo, H., Wang, X., & Ai, S. (2023). Exploring surface-enhanced Raman spectroscopy (SERS) characteristic peaks screening methods for the rapid determination of Chlorpyrifos residues in Rice. *Applied Spectroscopy, 77*(2), 160–169. https://doi.org/10.1177/00037028221141728

Xu, Q., Guo, X., Xu, L., Ying, Y., Wu, Y., Wen, Y., & Yang, H. (2017). Template-free synthesis of SERS-active gold nanopopcorn for rapid detection of chlorpyrifos residues. *Sensors and Actuators B: Chemical, 241*, 1008–1013. https://doi.org/10.1016/j.snb.2016.11.021

Ye, Z. H., Chen, X. T., Zhu, H. Y., Liu, X. Q., Deng, W. H., Song, W., & Peng, C. Y. (2023). Aggregating-agent-assisted surface-enhanced Raman spectroscopy-based detection of acrylamide in fried foods: A case study with potato chips. *Food Chemistry, 403*, Article 134377. https://doi.org/10.1016/j.foodchem.2022.134377

Zhang, C., Chen, S., Jiang, Z., Shi, Z., Wang, J., & Du, L. (2021). Highly sensitive and reproducible SERS substrates based on ordered micropyramid Array and silver nanoparticles. *ACS Applied Materials & Interfaces, 13*(24), 29222–29229. https://doi.org/10.1021/acsami.1c08712

Zhang, D., You, H., Yuan, L., Hao, R., Li, T., & Fang, J. (2019). Hydrophobic slippery surface-based surface-enhanced Raman spectroscopy platform for ultrasensitive detection in food safety applications. *Analytical Chemistry, 91*(7), 4687–4695. https://doi.org/10.1021/acs.analchem.9b00085

Zhao, T., Liang, X., Guo, X., Yang, X., Guo, J., Zhou, X., & Zhou, H. (2023). Smartphone-based colorimetric sensor array using gold nanoparticles for rapid distinguishment of multiple pesticides in real samples. *Food Chemistry, 404*, Article 134768. https://doi.org/10.1016/j.foodchem.2022.134768

Zhu, J., Agyekum, A. A., Kutsanedzie, F. Y. H., Li, H., Chen, Q., Ouyang, Q., & Jiang, H. (2018). Qualitative and quantitative analysis of chlorpyrifos residues in tea by surface-enhanced Raman spectroscopy (SERS) combined with chemometric models. *Lwt, 97*, 760–769. https://doi.org/10.1016/j.lwt.2018.07.055

Zook, J. M., Maccuspie, R. I., Locascio, L. E., Halter, M. D., & Elliott, J. T. (2011). Stable nanoparticle aggregates/agglomerates of different sizes and the effect of their size on hemolytic cytotoxicity. *Nanotoxicology, 5*(4), 517–530. https://doi.org/10.3109/17435390.2010.536615

Zrimsek, A. B., Chiang, N., Mattei, M., Zaleski, S., McAnally, M. O., Chapman, C. T., … Van Duyne, R. P. (2017). Single-molecule chemistry with surface- and tip-enhanced Raman spectroscopy. *Chemical Reviews, 117*(11), 7583–7613. https://doi.org/10.1021/acs.chemrev.6b00552